Tunable high-Q photonic-bandgap Fabry–Perot resonator

Jiu Hui Wu, Lay Kee Ang, Ai Qun Liu, Hwee Gee Teo, and Chao Lu

School of Electrical and Electronic Engineering, Nanyang Technological University, Nanyang Avenue, Singapore 639798

Received September 22, 2004; revised manuscript received December 21, 2004; accepted March 1, 2005

We report a theoretical analysis of a two-dimensional silicon photonic-bandgap (PBG) structure with ten layers of air-filled circular holes and an air-filled line defect, to function as a Fabry–Perot (FP) resonator. Using a multiple propagation series method, our calculations have shown a group of nine or ten resonant peaks of high-quality-factor Q (>2000) and of equal spacing (>80 nm) between two photonic bandgaps. The resonant peaks have large tunability in wavelength by varying the incident angle of light, which can be continuously tuned from 1.23 to 2.08 μm. The Q values of the resonant peaks increase linearly at small incidence and sharply at large incidence. For a lossy medium, the Q values may decrease significantly at large incidence angles, but resonant frequencies are relatively unchanged. The applications of the proposed PBG FP resonator for wavelength-division-multiplexed optical communications are discussed.

OCIS codes: 230.5750, 260.5740, 050.2230.

1. INTRODUCTION

With the recent advances in wavelength division multiplexing (WDM) systems, optical networks have progressed from single-wavelength point-to-point data links to fully reconfigurable multiple-wavelength systems. Wavelength demultiplexers are playing an important role in enhancing the capacity of optical communications. Fiber Bragg gratings,[1] arrayed waveguide gratings,[2] and cascaded Mach–Zehnder filters[3] are excellent devices for filtering purposes, but their sizes are on the order of centimeters or larger to support a large number of sufficiently spaced wavelength channels.

The emerging technology of photonic crystals can be suitably exploited to design novel optical devices for WDM applications. Because of the potentials of optical-device miniaturization, photonic-crystal-based wavelength demultiplexers have received great attention recently.[4–10] Various photonic-crystal-based properties have been proposed, including the channel-drop tunneling scheme,[4–6] the superprism effect,[7] and the frequency-selective dropping of photons from waveguide channel to the surrounding media.[8–10] These compact configurations all involve the interactions of waveguides with microcavities and therefore require detailed tunings of the cavity properties, which represents a challenge in design and fabrication.

In general, WDM application requires considerably high device performance, such as high filtering resolution, high out-of-band rejection, and high coupling efficiency with external optics. Over the past few years, several studies have been done to improve the quality (Q) factors of those filters by creating defect cavities inside a photonic-crystal structure.[11,12] By applying fractional dislocation geometry, the Q factor could be increased to values as high as 2800 (Ref. 13). Meanwhile, by adopting a donor-type point defect with three missing holes of linear shape, the Q factor of the surface-emitting-type channel-drop filter theoretically increases to values as high as 2900 (Ref. 14).

In this paper, we propose a simple two-dimensional photonic-bandgap (PBG) structure with an air-filled line defect ($\varepsilon_d = 1$) to function as a Fabry–Perot (FP) resonator (see Fig. 1). The FP resonator has two identical PBG slabs composed of a rectangular array of air-filled circular holes ($\varepsilon_a = 1$) in a silicon background ($\varepsilon_b = 12.1$). This PBG structure is different from the previous studies of a system of arrayed cylinders ($\varepsilon_a = 10$) with a line defect as a resonant cavity, and the dielectric constants of the defect and the background are equal ($\varepsilon_d = \varepsilon_b = 1$),[15] which has been studied by use of the layer-doubling method based on the scattering-matrix method.[16,17] For our PBG structure as shown in Fig. 1, we have $\varepsilon_a = \varepsilon_d \neq \varepsilon_b$ condition that the layer-doubling method cannot be applied directly. Here a simple multiple propagation series (MPS) method is used to calculate the transmittance as a function of incidence angle by superposing the successive transmissions–reflections series from the two slabs. With the MPS method, the setting of the structure is optimized to produce a group of nine or ten resonant peaks of high Q, which can be continually tuned to cover a very large frequency range by simply changing the incident angle. It is expected that the important characteristics presented in this paper can be applied to channel add–drop filters and–or wavelength monitoring devices for WDM optical communications.

The paper is organized as follows: We first introduce the PBG structure and the MPS method we use in Section 2. In Section 3, we first present our calculations, which

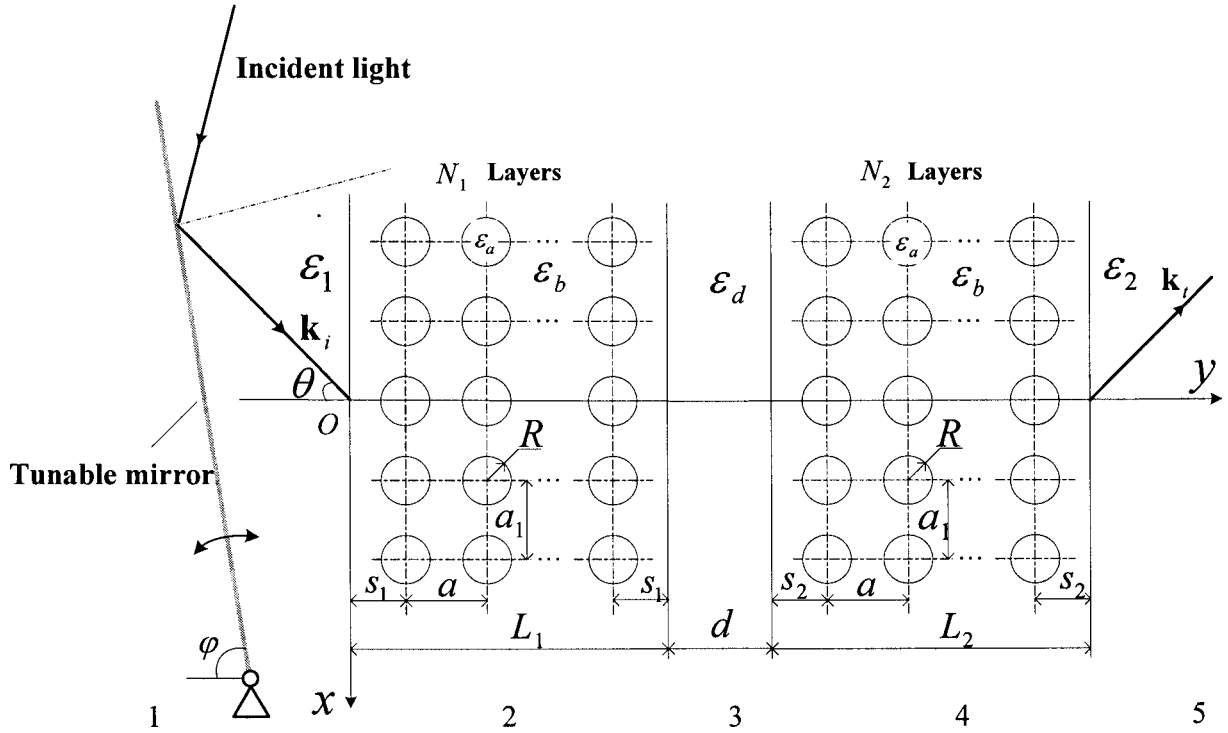

Fig. 1. Schematic presentation of the studied 2D PBG structure with a linear air defect. An external mirror is rotated to change the incident angle of light so that the transmission spectra can be continuously tuned to cover a very large frequency range.

agree well with finite difference time domain (FDTD) simulation on normal incidence. By varying the incident angles, we show the tunability of the resonance spectra and increment of Q for both lossless and lossy medium. Finally, the transmittance at various settings such as R, s, and N are discussed. The paper is summarized in Section 4.

2. THE PHOTONIC-BANDGAP STRUCTURE AND MULTIPLE-PROPAGATION-SERIES METHOD

Consider that two lattice slabs composed of a rectangular array of circular rods divide the 2D $x-y$ plane into five regions, as shown in Fig. 1. An external mirror in region 1 is used to tune continuously the incident angle θ of the incoming plane wave with wave number $\mathbf{k}_i=(k_1 \sin\theta, k_1 \cos\theta)$, and a outgoing wave is transmitted in region 5 with wave number $\mathbf{k}_t$, where the dielectric constants in regions 1 and 5 are $\varepsilon=\varepsilon_1$ and $\varepsilon=\varepsilon_2$, respectively. In regions 2 and 4, there are N_1 and N_2 layers of circular rods of radius R, which has a dielectric constant of $\varepsilon=\varepsilon_a$, embedded in a background lattice of $\varepsilon=\varepsilon_b$. The periodical spacings between the rods are a and a_1 in the y and x directions. The two slabs are separated by a defect region that has a uniform $\varepsilon=\varepsilon_d$ and a width of d. The distances from the defect's boundary to the nearest circular rods are s_1 and s_2. The thicknesses of the two slabs are $L_1=(N_1-1)a+2s_1$ and $L_2=(N_2-1)a+2s_2$, respectively.

By assuming that the two lattice slabs are independent of each other, the transmission (reflection) spectra of the two slabs in regions 2 and 4 can be calculated using Sakoda's method,[18] or other methods. When the incident wave is in a different region, the transmission (reflection) spectra are different, which are denoted by $T_2^{(1)}$, $T_2^{(3)}$, and $T_4^{(3)}$ ($R_2^{(1)}$, $R_2^{(3)}$ and $R_4^{(3)}$), respectively, with the superscript showing the incident region and the subscript (2 or 4) denoting either the first or second slab in region 2 and 4, respectively. To determine the final transmission T (or reflection R) of the system, MPS method is used to add up all the possible paths during the light propagation, such as $T=T^{(1)}+T^{(2)}+T^{(3)}+\cdots$, and $R=R^{(1)}+R^{(2)}+R^{(3)}+\cdots$, as shown in Figs. 2(a) and 2(b). In the figures, each arrow represents a propagation term in a uniform medium, and each circle of T or R represents the "response" (either transmission or reflection) for a single and independent slab. As an example, in Fig. 2(a), $T^{(1)}:T_2^{(1)}\rightarrow T_4^{(3)}$ describes the first transmission path without any reflection, which is defined by $T_2^{(1)}$ and $T_4^{(3)}$. $T^{(2)}:T_2^{(1)}\rightarrow R_4^{(3)}\rightarrow R_2^{(3)}\rightarrow T_4^{(3)}$ denotes the second transmission path with two internal reflection events $R_4^{(3)}$ and $R_2^{(3)}$ occurred in the defect region. $T^{(3)}:T_2^{(1)}\rightarrow R_4^{(3)}\rightarrow R_2^{(3)}\rightarrow R_4^{(3)}\rightarrow R_2^{(3)}\rightarrow T_4^{(3)}$ is the third transmission path with four internal reflection events.

Thus the $T^{(1)}$ term can be expressed as

$$T^{(1)}=\sum_{n_1} T_{n_1,2}^{(1)} \exp(i\mathbf{k}_3^{(n_1)}\cdot\mathbf{d}^{(n_1)}+ik_{3,y}^{(n_1)}L_1) \times\sum_{n_2} T_{n_2,4}^{(3)} \exp(ik_{5,y}^{(n_1,n_2)}L_2), \quad (1)$$

where $\mathbf{d}^{(n)}=(k_{3,x}^{(n)}d/k_{3,y}^{(n)},d)$, n_1 and n_2 are dummy integers from $-\infty$ to ∞, and $\mathbf{k}_3^{(n_1)}$ and $\mathbf{k}_5^{(n_1,n_2)}$ are the transmitted Bragg wave vectors in regions 3 and 5, respectively, which are given by

$$k_{3,x}^{(n_1)} = k_1 \sin\theta + 2\pi n_1/a_1; \tag{2}$$

$$k_{5,x}^{(n_1,n_2)} = k_1 \sin\theta + 2\pi(n_1+n_2)/a_1; \tag{3}$$

$$k_{3,y}^{(n_1)} = \begin{cases} [k_3{}^2 - (k_{3,x}^{(n_1)})^2]^{1/2} & \text{if } k_3 \geqslant |k_{3,x}^{(n_1)}|, \\ i[(k_{3,x}^{(n_1)})^2 - k_3{}^2]^{1/2} & \text{otherwise;} \end{cases} \tag{4}$$

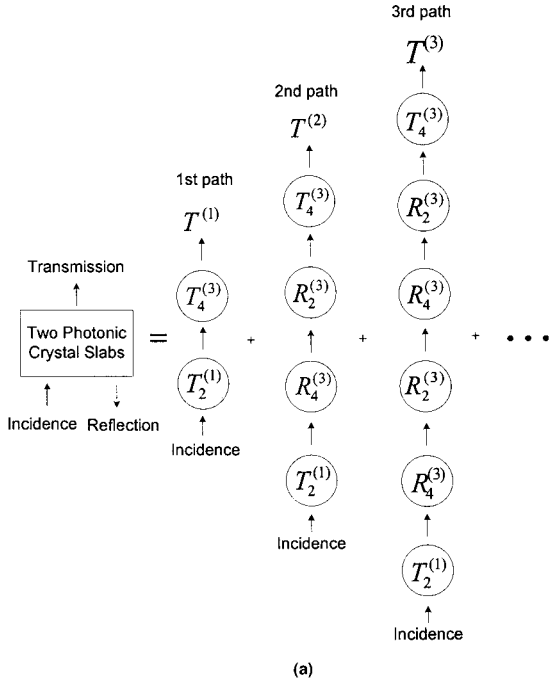

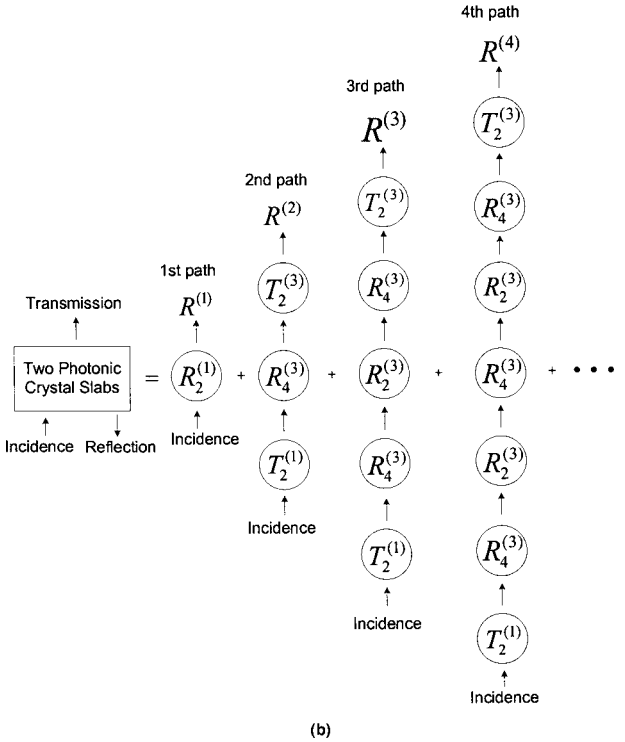

Fig. 2. Diagram of the MPS: (a) Transmission T, and (b) Reflection R.

$$k_{5,y}^{(n_1,n_2)} = \begin{cases} [k_5{}^2 - (k_{5,x}^{(n_1,n_2)})^2]^{1/2} & \text{if } k_5 \geqslant |k_{5,x}^{(n_1,n_2)}|, \\ i[(k_{5,x}^{(n_1,n_2)})^2 - k_5{}^2]^{1/2} & \text{otherwise;} \end{cases} \tag{5}$$

where $k_1=\sqrt{\varepsilon_1}\omega/c$, $k_3=\sqrt{\varepsilon_d}\omega/c$, and $k_5=\sqrt{\varepsilon_2}\omega/c$, ω is the angular frequency of the incident field, and c is the speed of light. Equations (2) and (3) reveal that every time light goes through a PBG slab, the x component of the Bragg wave vector will be changed by an integer multiple of $2\pi/a_1$ as a "response" to either transmission or reflection. By rewriting $n_1+n_2=n_2' \to n_2$, Eq. (1) becomes

$$T^{(1)} = \sum_{n_1,n_2} T_{n_1,2}^{(1)} \exp(i\mathbf{k}_3^{(n_1)} \cdot \mathbf{d}^{(n_1)} + ik_{3,y}^{(n_1)} L_1) \cdot T_{n_2-n_1,4}^{(3)} \times \exp(ik_{5,y}^{(n_2)} L_2), \tag{6}$$

where $\Sigma_{n_1,n_2}=\Sigma_{n_1}\Sigma_{n_2}$.

For any transmission path k, the general expression is

$$T^{(k)} = \sum_{n_1,\cdots,n_{2k}} \left\{ T_{n_1,2}^{(1)} \exp\left[\sum_{j=1}^{2k-1} i\mathbf{k}_3^{(n_j)} \cdot \mathbf{d}^{(n_j)} + ik_{3,y}^{(n_1)} L_1 + ik_{5,y}^{(n_{2k})} L_2 \right] \cdot T_{n_{2k}-n_{(2k-1)},4}^{(3)} \cdot \prod_{j=2}^{k} [R_{n_{2j-2}-n_{2j-3},4}^{(3)} \cdot R_{n_{2j-1}-n_{2j-2},2}^{(3)}] \right\}. \tag{7}$$

Here, the dummy variables n_1 and n_{2k} correspond to the transmission response, and $n_2,\cdots,n_{2k-1}$ in $\Pi_{j=2}^{k}[R_{n_{2j-2}-n_{2j-3},4}^{(3)} \cdot R_{n_{2j-1}-n_{2j-2},2}^{(3)}]$ correspond to the multiple reflection events of $2(k-1)$ times.

Similarly, for reflection path, the expression is

$$R^{(1)} = \sum_{n_1} R_{n_1,2}^{(1)}, \tag{8}$$

$$R^{(k)} = \sum_{n_1,\cdots,n_{2k-1}} \left(T_{n_1,2}^{(1)} \exp\left\{ \sum_{j=1}^{2(k-1)} i\mathbf{k}_3^{(n_j)} \cdot \mathbf{d}^{(n_j)} + i[k_{3,y}^{(n_1)} + k_{1,y}^{(n_{(2k-1)})}] L_1 \right\} \cdot R_{n_2-n_1,4}^{(3)} \cdot T_{n_{(2k-1)}-n_{(2k-2)},2}^{(3)} \cdot \prod_{j=2}^{k-1} [R_{n_{2j-1}-n_{2j-2},2}^{(3)} \cdot R_{n_{2j}-n_{2j-1},4}^{(3)}] \right), \qquad (k=2,3,\cdots). \tag{9}$$

Every term in Eq. (9) represents multiple reflection events of $2k-3$ times between the two PBG configurations. For example, the second ($k=2$) and third ($k=3$) terms represent the single- and triple-reflection events, respectively.

In order to add all terms at O (the original point in Fig. 1), the vibration phase of all waves must be adjusted accordingly so that the phase $\Sigma_{j=1}^{2k-1} k_{3,x}^{(n_j)} \cdot d_x^{(n_j)} + k_{3,y}^{(n_1)} L_1 + k_{3,y}^{(n_1)} d + k_{5,y}^{n_{2k}} L_2$ is correspondingly reduced from the vibration phase of the transmission series $T^{(k)}$ ($k=1,2,\cdots$), and the phase $\Sigma_{j=1}^{2(k-1)} k_{3,x}^{(n_j)} \cdot d_x^{(n_j)}$ is reduced from the reflection series $R^{(k)}$ ($k=2,3,\cdots$). By summing all terms of the transmission and reflection, MPS gives

$$T=\sum_{k=1}^{\infty}\left\{\sum_{n_1,\cdots,n_{2k}} T^{(1)}_{n_1,2}\exp\left[\sum_{j=2}^{2k-1} ik^{(n_j)}_{3,y}\cdot d\right]\cdot T^{(3)}_{n_{2k}-n_{(2k-1)},4}\cdot\prod_{j=2}^{k}[R^{(3)}_{n_{2j-2}-n_{2j-3},4}\cdot R^{(3)}_{n_{2j-1}-n_{2j-2},2}]\right\}, \tag{10a}$$

$$R=\sum_{n_1} R^{(1)}_{n_1,2}+\sum_{k=2}^{\infty}\left\{\sum_{n_1,\cdots,n_{2k-1}} T^{(1)}_{n_1,2}\exp\left[\sum_{j=1}^{2(k-1)} ik^{(n_j)}_{3,y}\cdot d+i(k^{(n_1)}_{3,y}+k^{(n_{(2k-1)})}_{1,y})L_1\right]\cdot R^{(3)}_{n_2-n_1,4}\cdot T^{(3)}_{n_{(2k-1)}-n_{(2k-2)},2}\cdot\prod_{j=2}^{k-1}[R^{(3)}_{n_{2j-1}-n_{2j-2},2}\cdot R^{(3)}_{n_{2j}-n_{2j-1},4}]\right\}, \tag{10b}$$

which depend only on a single slab's transmission and reflection coefficients: $T_2^{(1)}$, $T_2^{(3)}$, $T_4^{(3)}$, $R_2^{(1)}$, $R_2^{(3)}$, and $R_4^{(3)}$, which can be calculated by various methods. Note that in this paper, we will use Sakoda's method to calculate them.

Without perforation, the PBG structure will degenerate into a FP model, and all dummy variables in Eqs. (10) vanish. For a special case that $k=k_1=k_3$ and $\varepsilon=\varepsilon_1=\varepsilon_2=\varepsilon_d=1.0$ (air), the transmission and reflection coefficients of plates 2 and 4 are $T_2=T_2^{(1)}=T_2^{(3)}$ and $R_2=R_2^{(1)}=R_2^{(3)}$, and $T_4=T_4^{(3)}$ and $R_4=R_4^{(3)}$, and Eqs. (10) become

$$T=\frac{T_2T_4}{1-R_4R_2\exp(2ikd\cos\theta)}, \tag{11a}$$

$$R=\frac{R_2+R_4[T_2{}^2\exp(2ikL_1\cos\theta)-R_2{}^2]\exp(2ikd\cos\theta)}{1-R_2R_4\exp(2ikd\cos\theta)}, \tag{11b}$$

which recover to the classical formula of a FP etalon.

It is important to note that the MPS method presented here is a generation of the Airy formulation for a FP interferometer. In terms of concepts, it is similar to the grating stacks method, which has been developed by use of a more rigorous mathematical formulation and implementation.[19–21]

3. SIMULATION RESULTS AND DISCUSSION

Using the MPS method, assuming that the input amplitude of the electric field is normalized to 1, we consider the transmittance $|T|^2$ for E polarization along the $\Gamma-X$ direction. With Eqs. (10), the transmission and reflection spectra can be calculated accurately and efficiently for the settings of the arbitrary parameters in such a PBG structure as a function of incident angle.

Considering a special system with the following parameters: $a=420$ nm, $a_1=0.6a$, $N_1=N_2=N=10$, $R=0.23a$, $\varepsilon_b=12.1$ (silicon), $\varepsilon_a=\varepsilon_d=1$ (air), $d=0.73a$, and $s_1=s_2=s=1.13a$, we first calculate the transmittance $|T|^2$ of normal incidence ($\theta=0$) as a function of normalized frequency $F=\omega a/2\pi c$ from $F=0.14$ to 0.37, as shown in Fig. 3(a), where the solid curve and dashed curve are, respectively, from the MPS method and the FDTD method (by use the commercial software RSoft). It is clear that the MPS method agrees very well with the FDTD calculation and thus verifies the MPS method presented here.

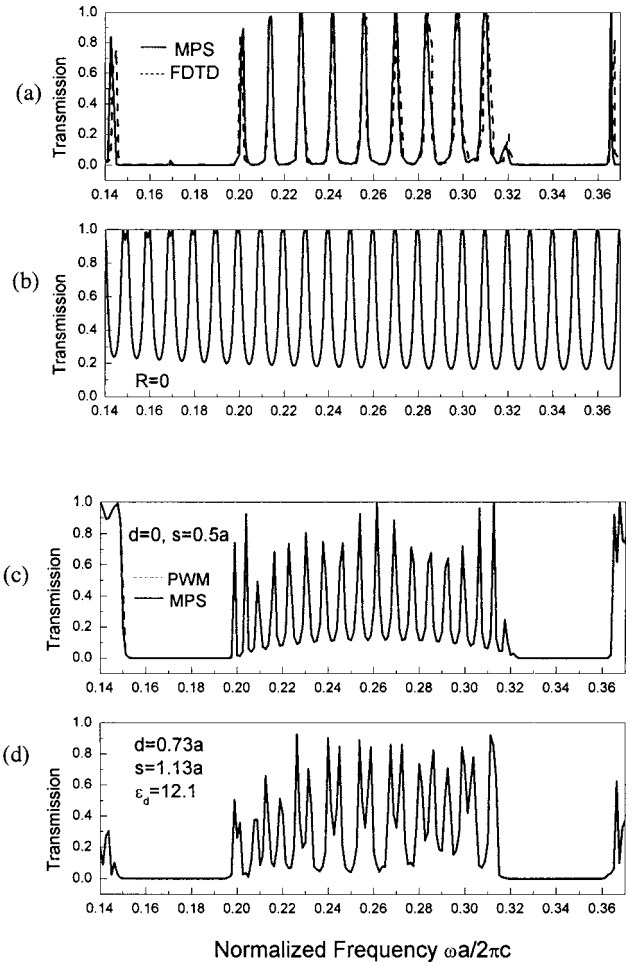

Fig. 3. Transmittance as a function of normalized frequency at $\theta=0°$, $N=10$, and $\varepsilon_a=1$ for four different settings $(R,s,d,\varepsilon_d,\varepsilon_b)$: (a) $(0.23a,1.13a,0.73a,1,12.1)$, (b) $(0,1.13a,0.73a,1,12.1)$, (c) $(0.23a,0.5a,0,1,12.1)$, and (d) $(0.23a,1.13a,0.73a,12.1,12.1)$. The solid curves are from MPS method, and the dashed curves are from (a) FDTD method, and (c) PWM method.

In Fig. 3(a), the spectra shows a group of nine transmittance (or resonant) peaks ($|T|^2\approx1$) at a center of the spectra between two photonic bandgaps. The peaks are of equal spacing and have moderate values of $Q=120-160$. The existence of the peaks is due to the combined effects of the PBG structures and the FP resonator, which are controlled by various parameters such as R, d, s, and ε_d. By varying these parameters, the corresponding transmittances are plotted in Figs. 3(b)–3(d) to illustrate the combined effects while the other parameters are unchanged.

In Fig. 3(b), the $R=0$ limit shows the spectra of a classical FP resonator, which has the transmittance bounded between 0.2 and 1. Without perforation ($R=0$), there is no bandgap in the spectra as expected. By setting $d=0$ and $s=0.5a$, the system becomes a simple periodic and defect-free photonic-crystal slab, which has two bandgaps at $F\approx0.15$ to $F\approx0.2$, and $F\approx0.32$ to $F\approx0.36$, as shown in Fig. 3(c). To introduce a simple line defect into the defect-free

photonic-crystal slab, we simply break the periodicity in the middle of the slab by setting $d=0.73a$, $s=1.13a$, and $\varepsilon_d=\varepsilon_b=12.1$. Figure 3(d) shows the transmittance of such a photonic-crystal slab with a simple geometrical defect, where the defect region and the PBG have the same dielectric constants ($\varepsilon_d=\varepsilon_b=12.1$). By comparing Figs. 3(c) and 3(d), we see that the widths of the two bandgaps are relatively unchanged, and both figures have various irregular transmission peaks ($|T|^2<1$) between the bandgaps. Since a classical FP shown in Fig. 3(b) is able to produce regular and high transmittance, we further introduce a new defect by varying $\varepsilon_d=12.1$ to $\varepsilon_d=1$ to obtain the nine resonant peaks ranging from $F\approx0.2$ to $F\approx0.31$, which are shown in Fig. 3(a). Note that there is a smaller peak (the tenth peak) at $F\approx0.32$, which will become dominant at large incidence angles (see Fig. 8 below).

From Fig. 3(a), we see that the nine transmission peaks bounded by the two bandgaps are created by a PBG-like FP resonator, which is composed of two silicon PBG slabs separated by an air-filled line defect. The resonant peaks are from the FP interference effects that occurred in the defect region of width d, which are modified by the PBG slabs. In addition, the purposes of the two PBG slabs are also used to create the two bandgaps and to suppress the transmittance at frequencies other than the resonant frequencies. From the classical FP interference theory, we know that large dielectric index contrast ($\varepsilon_b=12.1>\varepsilon_d=1$) is required to obtain high reflectivity between air and silicon, and this explains the large transmittance at higher Q obtained in Fig. 3(a) as compared with those obtained in Fig. 3(d) using $\varepsilon_b=\varepsilon_d=12.1$.

Our calculations are based on the MPS method presented in Section 2, which allows efficient and accurate calculations to obtain suitable settings of any arbitrary values of R, d, s, ε_d, N, and θ, in order to design a PBG-like FP resonator for high transmittance and high Q. In our calculation, a cutoff value of $k=4$ [see Eqs. (10)] with 3780 Fourier components has been used to ensure sufficient convergence and accuracy. More importantly, the calculations have been verified by use of both the FDTD method in Fig. 3(a) and the conventional plane-wave method (PWM)[18,22] in Fig. 3(c), which are both plotted in dashed curve. Both comparisons show excellent agreements, even for such a PBG FP system with a finite thickness and a large dielectric index contrast, as studied in this paper.

To increase further the Q values (obtained at normal incidence), we may increase the incidence angles (θ) to increase the reflectivity and thus the values of Q. This can be analogous to a symmetrical FP interferometer[23,24] in which $Q\propto R/(1-R^2)$. Figure 4 shows the two of the resonant peaks at various incidences: $\theta=0°$, 45°, 85°, and 89°. For a fixed θ, the spectra may contain either nine (small θ) or ten (large $\theta>75°$) resonant peaks with nearly equal spacing. Here, only the fifth (left) and sixth (right) resonant peaks are plotted, which correspond to wavelength $\lambda=1.55$ μm at a normalized frequency of $F\approx0.27097$. From the figure, we see that very high Q ($>10^4$) can be obtained at oblique incidence of $\theta\geqslant85°$. The central frequency of the peak is also continuously tuned from 0.26969 to 0.28565 (1.557 μm to 1.47 μm) with an increasing of θ.

Figure 5 reveals the dependence of the resonant frequency and the quality factor Q as a function of incidence angle for the sixth resonant peak propagating in both lossless and lossy PBG structures. Here, the symbols (Δ) and (∇) represent the resonant frequencies at $\varepsilon_b=12.1$ and $\varepsilon_b=12.1+0.01i$, and the symbols ($\cdot$), ($\bullet$), and ($\circ$) represent the Q factor at $\varepsilon_b=12.1$, $\varepsilon_b=12.1+0.01i$, and $\varepsilon_b=12.1+0.001i$, respectively. Here the imaginary parts of

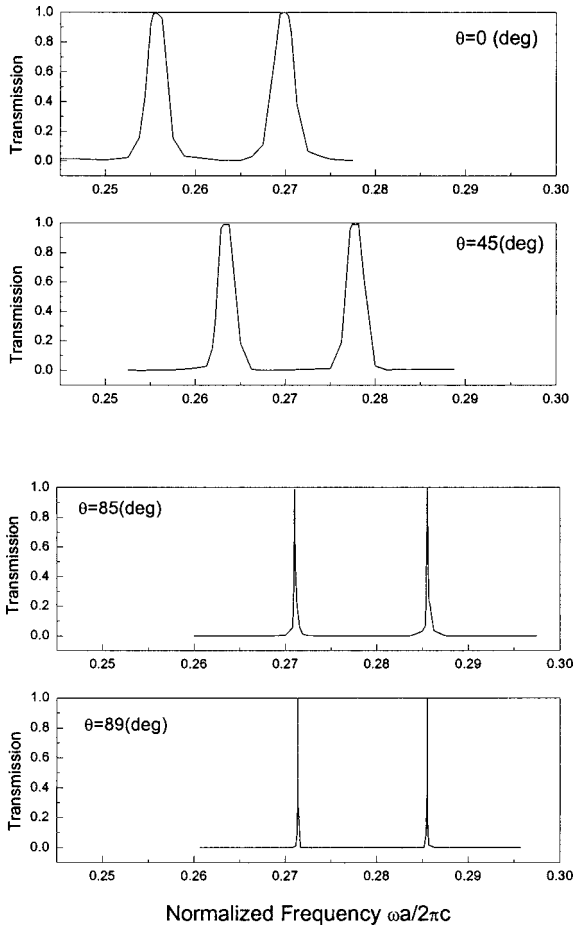

Fig. 4. Continuous tunability of the fifth and sixth resonant peaks of the 2D PBG FP resonator for increasing incident angle: $\theta=0°$ (top) to $\theta=89°$ (bottom).

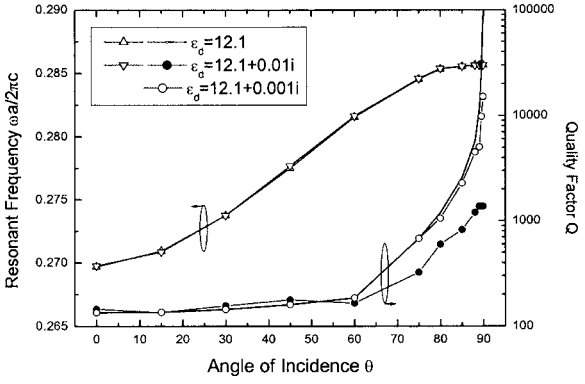

Fig. 5. Resonant frequency and quality factor of the sixth resonant peak as a function of θ (up to 89.9°) for three dielectric medium: $\varepsilon_b=12.1$, $\varepsilon_b=12.1+0.01i$, and $\varepsilon_b=12.1+0.001i$.

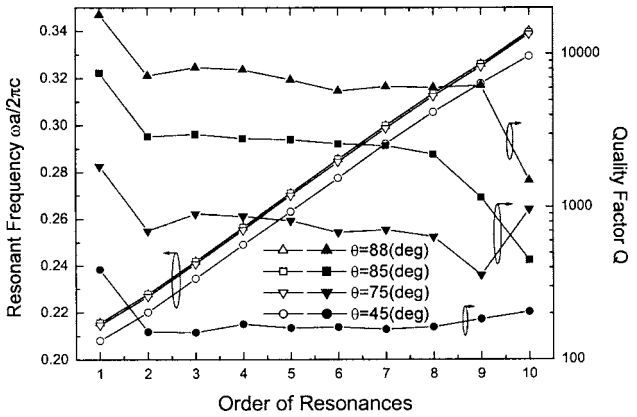

Fig. 6. Resonant frequency and quality factor for the ten resonant peaks at four incident angles (θ=45°, 75°, 85°, and 88°).

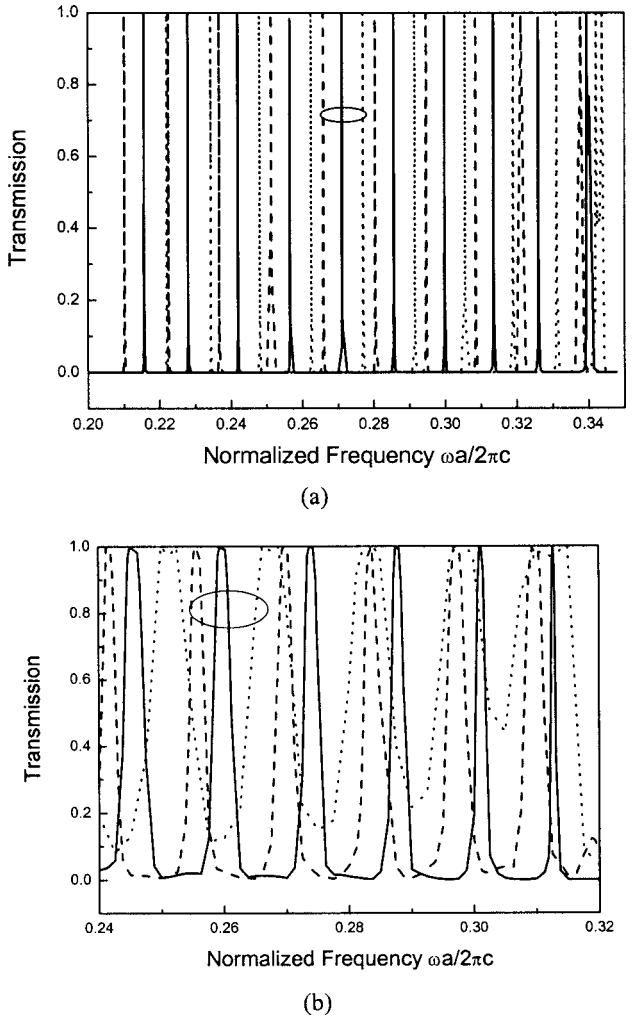

Fig. 7. Transmittance for (a) R/a=0.22, 0.23, and 0.24 (left to right) at θ=88°; and (b) s/a=0.3, 1, and 1.13 (right to left) at θ=0°.

the dielectric constants are assumed according to Ref. 17. Independent of ε_b, the resonant frequency can be tuned almost linearly from 0.27 to 0.28565 over a wide range of θ. For a lossless dielectric, the quality Q (<200) remains relatively small for small θ (0° to 60°), and it increases sharply up to $Q=10^5$ at θ=89.9°. However, by including the loss tangent of the dielectric constant, the calculated Q values are significantly limited at the large θ. For $\varepsilon_b=12.1+0.01i$ case, the Q values can be decreased by a factor of 100 as compared with the ε_b=12.1 case, as shown in the figure. It is a matter of course that a larger imaginary part leads to a smaller quality factor. It should be noticed that the Q value is limited by the loss tangent of the dielectric material but not by the PBG structure itself.

In Fig. 6, we show the resonant frequency and the Q factor for all ten resonant peaks without the dielectric loss (ε_b=12.1) at four different incident angles (θ=45°, 75°, 85°, and 88°). We found that the adjacent peaks are separated from each other with a constant normalized spacing of ΔF=0.0142, which is independent of θ. When θ increases from 0° to ~90°, every resonant peak is tuned with about ΔF=0.014, and thus, the entire group of nine transmission peaks may completely cover a large frequency range from F=0.20157 to F=0.34. Thus, by changing θ with the mirror as shown in Fig. 1, the proposed PBG-like FP resonator can be tuned over a large range: λ=1.23 to 2.08 μm (with a=420 nm assumed in this calculation). Note the frequencies (of all ten peaks) are identical from θ=75°, 85°, and 88°, which indicates that the tunability saturates at large incident angles as shown in

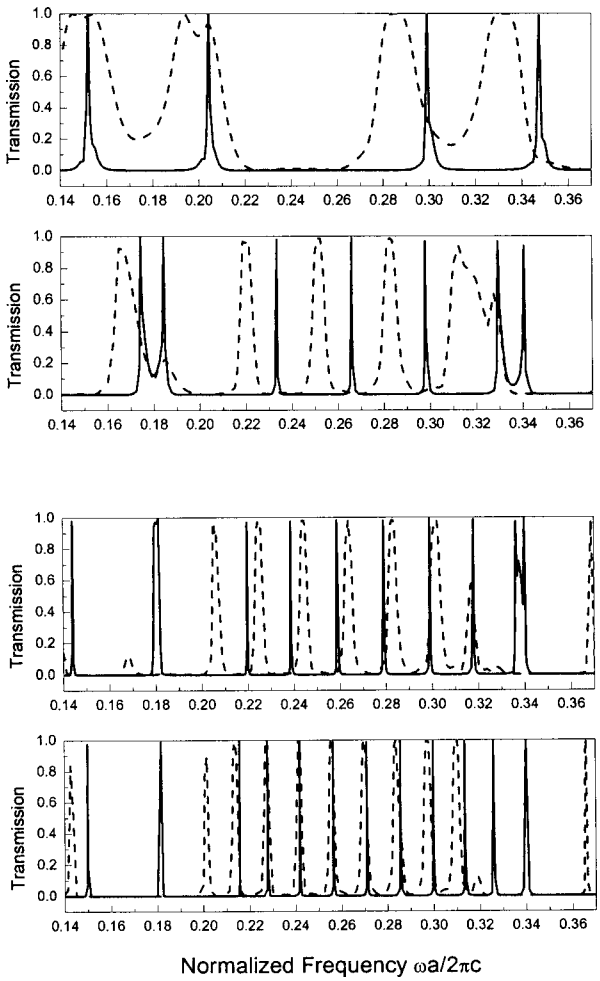

Fig. 8. Transmittance for different N=1, 4, 7, and 10 (top to bottom) for θ=85° (solid curves) and θ=0° (dashed curves).

Figs. 5 and 6. Figure 6 also shows that $Q>2000$ at $\theta \geqslant 85°$ for all resonant peaks, except for the last two peaks for a lossless PBG FP resonator.

It is also of interest to see the sensitivity of the resonant spectra around the chosen values of $R=0.23a$ and $s=1.13a$. Figure 7(a) shows the transmission spectra of the resonant peaks for $R/a=0.22$, 0.23, and 0.24 (left to right) at $\theta=88°$, where the fifth resonant peaks have been highlighted. Decreasing R shifts the spectrum to lower frequencies, which can be explained by the change of an effective refractive index, as these changes will reduce the amount of lower dielectric material (in this case, air) with respect to higher dielectric material (in this case, silicon). Thus the effective refractive index increases and shifts the spectrum to lower frequencies. In Fig. 7(b), the transmittance spectra for $s/a=0.3$, 1, and 1.13 (right to left in the highlighted peaks) at $\theta=0°$ are plotted from $F=0.24$ to $F=0.32$. Thus the figure shows that a sufficiently large value of $s>R$ is required to obtain low rejection and high Q (i.e., $s=1.13a$ and $R=0.23a$), such that the circular holes in PBG slabs are far away from the defect region. For example, Q at $s=a$ is larger than Q at $s=0.3a$.

Finally, we vary the layer numbers N, and the transmittances for various $N=1$, 4, 7, and 10 at $\theta=85°$ (solid curves), and $\theta=0°$ (dashed curves) are plotted in Fig. 8. We see the number of the resonant peaks increase with N when the length of the FP resonator is larger. The Q values at high incidence ($\theta=85°$) are significantly larger than at normal incidence, especially when N is small.

From our calculations, we have shown that these resonance peaks with high Q have a fixed interval of larger than 80 nm, which is sufficient for WDM applications that normally require a spacing of ~30 nm. In addition, high attenuation (rejection depth >120 dB) and high coupling efficiency (almost 100%) are also revealed. Thus the proposed PBG-FP resonator may be useful for WDM optical communications where low-cost and highly efficient linear and nonlinear devices are currently in great demand. It is expected that the proposed high Q and tunable PBG-FP resonator can be fabricated with microelectromechanical systems technology.[25,26]

4. CONCLUSIONS

In this paper, we theoretically investigated the transmittance of a 2D PBG as a FP resonator for E polarization light at various incident angles. Using a MPS method, we efficiently determine a suitable setting, which provides nine or ten resonant peaks of high Q in a spectra region bounded by two PBGs. The resonant peaks are of equal spacing and can be continuously tuned to cover a large frequency range by increasing the incident angle. The Q factor of every resonant peak is extremely high at large incident angles for a lossless medium. The calculated Q values are extremely sensitive to the loss tangent of the dielectric, but the resonant frequency is relatively insensitive. Our calculations of the MPS method have also been verified with the FDTD method.

A. Q. Liu is the corresponding author and can be reached by telephone at (65) 6790-4336, by fax at (65) 6793-3318, or e-mail at eaqliu@ntu.edu.sg.

REFERENCES

1. Q. Mao and J. W. Y. Lit, "Widely tunable L-band erbium-doped fiber laser with fiber Bragg gratings based on optical bistability," Appl. Phys. Lett. **82**, 1335–1337 (2003).
2. T. Katchalski, E. Teitelbaum, and A. A. Friesem, "Towards ultranarrow bandwidth polymer-based resonant grating waveguide structures," Appl. Phys. Lett. **84**, 472–474 (2004).
3. T. A. Cusick, S. Iezekiel, R. E. Miles, S. Sales, and J. Capmany, "Synthesis of all-optical microwave filters using Mach–Zehnder lattices," IEEE Trans. Microwave Theory Tech. **45**, 1458–1462 (1997).
4. S. Fan, P. R. Villeneuve, and J. D. Joannopoulos, "Channel drop tunneling through localized states," Phys. Rev. Lett. **80**, 960–963 (1998).
5. S. Fan, P. R. Villeneuve, J. D. Joannopoulos, M. J. Khan, C. Manolatou, and H. A. Haus, "Theoretical analysis of channel drop tunneling processes," Phys. Rev. B **59**, 15882–15892 (1999).
6. C. Manolatou, M. J. Khan, S. Fan, P. R. Villeneuve, H. A. Haus, and J. D. Joannopoulos, "Coupling of modes analysis of resonant channel add-drop filters," IEEE J. Quantum Electron. **35**, 1322–1331 (1999).
7. S. Noda, A. Chutinan, and M. Imada, "Trapping and emission of photons by a single defect in a photonic bandgap structure," Nature **407**, 608–610 (2000).
8. A. Chutinan, M. Mochizuki, M. Imada, and S. Noda, "Surface-emitting channel drop filters using single defects in two-dimensional photonic crystal slabs," Appl. Phys. Lett. **79**, 2690–2692 (2001).
9. C. Jin, S. Fan, S. Han, and D. Zhang, "Reflectionless multichannel wavelength demultiplexer in a transmission resonator configuration," IEEE J. Quantum Electron. **39**, 160–165 (2003).
10. H. Kosaka, T. Kawashima, A. Tomita, M. Notomi, T. Tamamura, T. Sato, and S. Kasakami, "Photonic crystals for micro lightwave circuits using wavelength-dependent angular beam steering," Appl. Phys. Lett. **74**, 1370–1372 (1999).
11. J. Vuckovic, M. Loncar, A. Scherer, and H. Mabuchi, "Design of photonic crystal microcavities for cavity QED," Phys. Rev. E **65**, 016608–016618 (2001).
12. H. Y. Ryu, S. H. Kim, H. G. Park, J. K. Hwang, Y. H. Lee, and J. S. Kim, "Square-lattice photonic band-gap single-cell laser operating in the lowest-order whispering gallery mode," Appl. Phys. Lett. **80**, 3883–3885 (2002).
13. T. Yoshie, J. Vuckovic, A. Scherer, H. Chen, and D. Deppe, "High quality two-dimensional photonic crystal slab cavities," Appl. Phys. Lett. **79**, 4289–4291 (2001).
14. Y. Akahane, M. Mochizuki, T. Asano, Y. Tanaka, and S. Noda, "Design of a channel drop filter by using a donor-type cavity with high-quality factor in a two-dimensional photonic crystal slab," Appl. Phys. Lett. **82**, 1341–1343 (2003).
15. S.-Y. Lin, V. M. Hietala, and S. K. Lyo, "Photonic band gap quantum well and quantum box structures: a high-Q resonant cavity," Appl. Phys. Lett. **68**, 3233–3235 (1996).
16. K. Sakoda, T. Ueta, and K. Ohtaka, "Numerical analysis of eigenmodes localized at line defects in photonic lattices," Phys. Rev. B **56**, 14905–14908 (1997).
17. T. Ueta, K. Ohtaka, N. Kawai, and K. Sakoda, "Limits on quality factors of localized defect modes in photonic crystals due to dielectric loss," J. Appl. Phys. **84**, 6299–6304 (1998).
18. K. Sakoda, "Optical transmittance of a two-dimensional triangular photonic lattice," Phys. Rev. B **51**, 4672–4675 (1995).
19. L. C. Botten, T. P. White, C. M. de Sterke, R. C. McPhedran, A. A. Asatryan, and T. N. Langtry, "Photonic crystal devices modelled as grating stacks: matrix generalizations of thin film optics," Opt. Express **12**, 1592–1604 (2004).
20. L. C. Botten, N. A. Nicorovici, A. A. Asatryan, R. C.

McPhedran, C. M. de Sterke, and P. A. Robinson, "Formulation for electromagnetic scattering and propagation through grating stacks metallic and dielectric cylinders for photonic crystal calculations. Part I. Method," J. Opt. Soc. Am. A **17**, 2165–2176 (2000).
21. L. C. Botten, N. A. Nicorovici, A. A. Asatryan, R. C. McPhedran, C. M. de Sterke, and P. A. Robinson, "Formulation for electromagnetic scattering and propagation through grating stacks metallic and dielectric cylinders for photonic crystal calculations. Part II. Properties and implementation," J. Opt. Soc. Am. A **17**, 2177–2190 (2000).
22. K. Sakoda, "Transmittance and Bragg reflectivity of two-dimensional photonic lattices," Phys. Rev. B **52**, 8992–9002 (1995).
23. H. M. Gibbs, *Optical Bistability: Controlling Light with Light* (Academic, 1985).
24. A. Yariv and P. Yeh, *Optical Waves in Crystals: Propagation and Control of Laser Radiation* (Wiley, 1984).
25. A. Q. Liu, X. M. Zhang, D. Y. Tang, and C. Lu, "Tunable laser using micromachined grating with continuous wavelength tuning," Appl. Phys. Lett. **85**, 3684–3686 (2004).
26. X. M. Zhang, A. Q. Liu, D. Y. Tang, and C. Lu, "Discrete wavelength tunable laser using microelectromechanical systems technology," Appl. Phys. Lett. **84**, 329–331 (2003).